Fuelling a solid oxide fuel cell with ammonia recovered from water by vacuum membrane stripping

van Linden, Niels; Spanjers, Henri; van Lier, Jules B.

DOI
10.1016/j.cej.2021.131081

Publication date
2022

Document Version
Final published version

Published in
Chemical Engineering Journal

Chemical Engineering Journal 428 (2022) 131081

Contents lists available at ScienceDirect

Chemical Engineering Journal

journal homepage: www.elsevier.com/locate/cej

Fuelling a solid oxide fuel cell with ammonia recovered from water by vacuum membrane stripping

Niels van Linden *, Henri Spanjers, Jules B. van Lier

Delft University of Technology, Faculty of Civil Engineering and Geosciences, Department of Watermanagement, Stevinweg 1, 2628 CN Delft, the Netherlands

ARTICLE INFO

Keywords:
Ammonia recovery
Ammonia stripping
Ammonia-water mixture
Energy generation
Vacuum membrane stripping
Solid oxide fuel cell

ABSTRACT

Gaseous ammonia (NH_3) recovered from residual waters may be used as a fuel in solid oxide fuel cells (SOFCs) to generate electricity without emission of undesirable oxidised nitrogen species. NH_3 can be directly recovered from water as a gas by vacuum membrane stripping (VMS), which also results in the evaporation of water (H_2O), leading to the recovery of NH_3-H_2O mixtures. However, in currently available literature, information is lacking on the NH_3 concentrations in NH_3-H_2O mixtures that may be used as a fuel for an oxygen-conducting SOFC (SOFC-O). In this study, we assessed the effect of feed water temperature and the NH_3 feed water concentration on the NH_3 concentrations in gaseous VMS permeate. Besides, we assessed the feasibility to use NH_3-H_2O mixtures in the concentration range between 5 and 25 wt% for the generation of electricity in an SOFC-O. The results show that increasing the NH_3 feed water concentration from 1 to 10 g·L^{-1} increased the NH_3 concentration in the gaseous VMS permeate from 1 wt% to up to 11 wt%. Increasing the feed water temperature from 25 to 35 °C also results in an increase in the NH_3 concentration in the gaseous permeate, whereas increasing the feed water temperature from 35 °C to 55 °C leads to dilution of the VMS permeate. Furthermore, electricity was generated at an electrical efficiency of 43% in an SOFC-O when the NH_3 concentration in the NH_3-H_2O fuel was only 5 wt%. Hence, according results on the obtained NH_3 concentrations in the gaseous VMS permeate and the generation of electricity using dilute NH_3-H_2O mixtures as a fuel, VMS and SOFC-O can be combined for the generation of electricity from NH_3 recovered from water. Moreover, the electrical energy generation of the SOFC-O, which reached values of 9 MJ·kg-N^{-1}, was higher than the electrical energy consumption for VMS, for which values of 7 MJ·kg-N^{-1} were calculated.

1. Introduction

1.1. Recovery of total ammoniacal nitrogen from water

Currently, biochemical treatment methods, such as nitrification–denitrification and partial nitritation in combination with anaerobic ammonium oxidation are commonly used to remove total ammoniacal nitrogen (TAN), which is the sum of the concentration of dissolved ammonium (NH_4^+) and ammonia (NH_3), from residual waters. However, recovery of TAN from residual streams that contain high (>0.5 g·L^{-1}) TAN concentrations, is currently receiving growing interest as an alternative to biochemical TAN destruction [1–3]. Examples of residual streams that contain high TAN concentrations are source-separated urine, industrial condensates and reject water, which is the liquid fraction of anaerobically digested waste activated sludge, manure or landfill leachate [3]. Recovery of TAN can be achieved via struvite precipitation by the addition of magnesium to residual waters that also contain phosphate, or by scrubbing stripped NH_3-containing off-gas that is obtained after chemical addition for pH increase, followed by air- or steam stripping in acid solutions [2]. Recovered products such as struvite, ammonium sulphate and ammonium nitrate are typically used as (a resource for the production of) fertiliser [1,2]. In addition, recovered TAN in the form of ammonia-water (NH_3-H_2O) mixtures can be used for carbon dioxide (CO_2) capture from flue gases [4]. However, recovery of NH_3 as a resource is not always desirable, because large amounts of chemicals and energy are typically required to drive the recovery technologies. Moreover, the use of the recovered products can be challenging due to legislation, quality restrictions, storage and transportation costs, and supply and demand mismatches [1,2].

* Corresponding author.
E-mail address: N.vanLinden@tudelft.nl (N. van Linden).

https://doi.org/10.1016/j.cej.2021.131081
Received 26 March 2021; Received in revised form 13 June 2021; Accepted 26 June 2021
Available online 3 July 2021

1.2. Use of gaseous ammonia for energy generation by using solid oxide fuel cells

The chemically stored energy in NH_3, which equals 21 MJ·kg-N^{-1}, referring to the lower heating value at 750 °C, can be converted to electricity and heat by various energy-conversion technologies [5]. NH_3 as energy source opens new opportunities for the application of recovered NH_3 from residual waters [3]. Whereas conventional combustion-based technologies initially convert the chemical energy to heat and subsequently generate electricity at efficiencies ranging between 30 and 40%, fuel cells allow for direct generation of electricity at up to 60% efficiency [6].

Amongst the various fuel cell types, three types are so-called direct NH_3 fuel cells: 1) alkaline fuel cells (AFCs), 2) alkaline membrane fuel cells (AMFCs) and 3) solid oxide fuel cells (SOFCs). According to review studies of Cheddie [7] and Lan et al. [8], the reported maximum (peak) power density of AFCs (16 mW·cm^{-2}) and AMFCs (40 mW·cm^{-2}) are an order of magnitude lower than the reported peak power density of SOFCs (ranging between 580 and 1,190 mW·cm^{-2}), using gaseous NH_3 directly as a fuel. Moreover, the use of AMFCs is challenged by catalyst poisoning by adsorbed N species at the anode, diffusion of NH_3 through the membrane electrolyte, and slow kinetics due to the low operating temperature (between 25 and 80 °C) [9]. Furthermore, the use of AFCs is challenged by carbonate formation in the liquid hydroxide electrolyte [8,10].

The high peak power densities of SOFCs are explained by the fast kinetics and the low resistances, as SOFCs operate at temperatures ranging between 600 and 1000 °C, allowing for electrical efficiencies up to 60% and total energy efficiencies up to 90% when the high-grade generated heat is used [6]. The operational temperature combined with the presence of nickel catalysts allows for spontaneous cracking of NH_3 to hydrogen (H_2) and N_2 (Eq. (1)) [11], without the need to change the materials or design of H_2-fuelled SOFCs to use NH_3 as a fuel [12]. SOFC types are distinguished based on their electrolyte properties [6,13]. SOFC-Os have an oxygen-conducting electrolyte, while SOFC-Hs have a proton-conducting solid electrolyte. In both types of SOFCs, cracking of NH_3 takes place at the anode. However, in SOFC-Os, oxygen (O_2) reduction to oxygen ions (O^{2-}) takes place at the cathode (Eq. (2)). Subsequently, O^{2-} transfer from the cathode to the anode allows for the reaction of O^{2-} with H_2 (Eq. (3)), resulting in the release of electrons. The electrons go through an electrical circuit to the cathode, allowing again for O_2 reduction. In contrast, in SOFC-Hs, protons (H^+) are formed at the anode and subsequent H^+ transfer takes place from the anode to the cathode. At the cathode, H^+ reacts with O_2, resulting in the release of electrons, which are again used at the anode to form H^+ from H_2. Currently, the reported peak power densities of SOFC-Os exceed the reported peak power densities of SOFC-Hs, due to optimal material selection and design of SOFC-Os as a result of extensive research [13,14]. Moreover, the conversion of NH_3 in SOFC-Os leads to very low emission of N-species. Dekker et al. [15] reported near-complete (>99.9%) cracking of NH_3 at the anode and only traces of NO_x (ranging between 0.5 and 4 ppm) in the anode off-gas of their SOFC-O. Research conducted by Staniforth et al. [11], Ma et al. [16] and Okanishi et al. [17] confirmed these findings and detected no NH_3, NO, NO_2 nor N_2O in the anode off-gas of their SOFC-O. Hence, SOFC-Os are potentially suitable to efficiently convert the chemically stored energy from recovered NH_3 to electricity, without the emission of undesirable oxidised N-species.

$$NH_3 + xH_2O \rightarrow 0.5N_2 + 1.5H_2 + xH_2O \quad (1)$$

$$0.75O_2 + 3e^- \rightarrow 1.5O^{2-} \quad (2)$$

$$1.5H_2 + 1.5O^{2-} \rightarrow (1.5 + x)H_2O + 3e^- \quad (3)$$

1.3. Direct gaseous ammonia recovery from water by vacuum membrane stripping

To allow for using the recovered NH_3 as a fuel for SOFC-Os, NH_3 must be extracted from the water phase as a gas. Hereto, vacuum stripping of NH_3 can be used, which avoids the presence of O_2 in the recovered gas. In contrast, applying air stripping will lead to deactivation of the nickel anode catalyst of SOFC-Os by oxidation of nickel to nickel oxide (NiO). The use of membranes in vacuum membrane stripping (VMS) configurations, results in large gas–liquid exchange areas in a small volume, allowing for compact systems. However, stripping of NH_3 from water is accompanied by the evaporation of H_2O, resulting in gaseous NH_3-H_2O mixtures in the VMS permeate. El-Bourawi et al. [18] and Ding et al. [19] studied the effects of the solution pH, feed water temperature, vacuum pressure, feed flow velocity, and feed water concentration NH_3 concentration on the NH_3 mass transfer coefficient, which relates the mass flux and the corresponding driving force. However, both studies did not report the effects on the individual transfer of NH_3 and H_2O, nor on the obtained NH_3 concentration in the recovered NH_3 stream. On the other hand, the studies of He et al. [20] and He et al. [21] reported concentrations of NH_3 in a range between 4 and 18 g-N·L^{-1} in the gaseous NH_3-H_2O mixtures recovered from biogas slurry by VMS, corresponding to a range between 0.5 and 2.2 wt% (weight %) of NH_3.

1.4. Direct use of recovered ammonia from water as a fuel for solid oxide fuel cells

To the best of our knowledge, only recent studies of Stoeckl et al. [22] and Stoeckl et al. [23] mentioned the use of recovered NH_3 as fuel for an SOFC-O. However, the authors used fuel with an NH_3 concentration of 70 wt%, as an NH_3-H_2O mixture, and did not mention for what kind of feed water and operating conditions this NH_3 concentration can be obtained. Hence, currently reported NH_3 concentrations, which are obtained by VMS (up to 2 wt%) and those that are used in NH_3-H_2O mixtures as fuel for SOFC-Os (70 wt%), do not match. This discrepancy makes it unclear whether VMS and SOFC-Os can be combined for the recovery of NH_3 from water and the subsequent direct use of the recovered NH_3 as a fuel. Therefore, more information is needed to bridge the gap in applicable NH_3 concentrations in NH_3-H_2O mixtures that can be obtained by VMS and directly be used by SOFC-O.

To obtain more concentrated NH_3-H_2O mixtures during the recovery of NH_3 by VMS, the amount of H_2O evaporated relative to the amount of NH_3 stripped must be minimized. In currently available literature on NH_3 recovery by VMS, feed water temperatures ranging between 40 and 75 °C are used [19–21,24,25]. All mentioned studies showed that when the feed water temperature increased, the NH_3 in the gaseous permeate was diluted. Therefore, VMS seems to be a suitable technology only for feed water temperatures below 40 °C. In addition, when increased NH_3 concentrations are present in the feed water, also the NH_3 flux increases [19,20,24,25]. Based on our previous research, NH_3 concentrations of 10 g·L^{-1} can be obtained, using electrodialysis to concentrate NH_4^+ [26], followed by chemical addition for pH increase. As an alternative for adding chemicals to obtain dissolved NH_3, bipolar membrane electrodialysis can be applied, which allows for the direct production of concentrated dissolved NH_3 without the addition of chemicals [27].

1.5. Research objectives

This study aimed to link VMS and SOFC-O for NH_3 recovery from water and to directly use the recovered NH_3 for electricity generation. The first goal of this study was to determine what NH_3 concentrations in the gaseous VMS permeate can be obtained for various feed water temperatures ranging between 25 and 55 °C. Experiments were performed with NH_3 feed water concentrations ranging between 1 and 10 g·L^{-1}, which is considered a relevant range for NH_3 recovery from residual waters. The second goal of this study was to determine the

required NH_3 concentrations for electricity generation in an SOFC-O, using dilute NH_3-H_2O mixtures, ranging between 5 and 25 wt%. In addition, we calculated the electrical energy consumption to recover NH_3 by VMS, as well as the energy generation of the SOFC-O using NH_3-H_2O mixtures as a fuel.

2. Materials and methods

2.1. Materials

2.1.1. Experimental vacuum membrane stripping set-up

For the VMS experiments, an acrylic Sterlitech flow-cell was used, containing a flat-sheet polytetrafluoroethylene (PTFE) hydrophobic membrane with polypropylene (PP) backing, having a pore size of 0.1 μm and a membrane area of 34 cm^2. A wire mesh spacer with a filament thickness of 0.8 mm and a void fraction of 91% was placed at the feed side to create the desired turbulence, while another wire mesh spacer was placed at the permeate side to avoid the membrane from sticking to the flow-cell.

The feed waters were stored in a 1 L borosilicate bottles and were recirculated through the flow-cell by a calibrated peristaltic Watson Marlow 520S pump equipped with Watson-Marlow 313 pump heads (0.3 – 46 $L{\cdot}h^{-1}$). A calibrated digital Festo IP40 pressure sensor (100 – 200,000 Pa) was used to measure the hydraulic pressure drop over the VMS flow-cell. The pH and electrical conductivity (EC) of the feed waters were continuously measured in the bottle, using a calibrated IDS SenTix 940 pH sensor and a calibrated TetraCon 925 EC-sensor, respectively. The data was automatically logged on a WTW Multi 3630 IDS multimeter and stored on a laptop. The feed water bottles were sealed during operation to avoid the loss of water and NH_3 from the feed water to the atmosphere. The feed water bottles were placed on an IKA RH Digital KT/C heating plate and magnetic stirrer combination, while an IKA Ikatron ETC 1 temperature sensor measured the temperature of the feed water and controlled the heating plate to maintain a stable feed water temperature. The heating-mixing combination and feed water bottle were placed on a Kern PCB 6000–1 mass balance (0.1 – 6,000 g) to continuously measure the total mass of the feed water. The data was automatically logged and stored on a laptop.

A calibrated KNF N816.3KT.45.18 vacuum pump was used to create a partial vacuum of 1,500 Pa at the permeate side of the membrane. The gaseous VMS permeate was scrubbed in a cooled acid trap containing 200 mL 1 M hydrochloric acid (HCl) solution (Merck), to protect the vacuum pump. Ammonium bicarbonate (NH_4HCO_3) (Sigma Aldrich Reagent Plus) and 1 M sodium hydroxide (NaOH) (Merck) was used to prepare the feed waters. Finally, the NH_3 concentrations in the feed waters were measured with Machery-Nagel NANOCOLOR 2,000 test kits (concentration range 0.4–2.0 $g{\cdot}L^{-1}$). Fig. 1 shows a schematic representation of the experimental VMS set-up.

2.1.2. Experimental solid oxide fuel cell set-up

For the SOFC-O experiments, a Fiaxell Open Flanges Set-up was used, which contained a 10 cm^2 planar anode-supported membrane electrode assembly (MEA). The MEA consisted of a NiO-8YSZ (nickel oxide coated zirconia stabilised by 8% yttria) anode, an O^{2-}-conducting 8YSZ electrolyte and a 20GDC-LSCF (lanthanum strontium cobalt ferrite stabilised by 20% gallium doped ceria) cathode. The MEA was sealed by a 0.5 mm thick mica sheet to limit the leakage of fuel from the anode to the cathode. At the anode, nickel foam with a thickness of 0.6 mm and a diameter of 40 mm was placed to provide extra surface area to crack NH_3. A golden mesh grid current collector was placed on top of the cathode to measure the electric potential and to draw electric current. Alumina sheets were placed at the cathode side of the MEA to avoid contact between the anode and cathode. The MEA and associating accessories were placed between a fuel and an air diffuser, both made of Inconel 601 (nickel–chromium alloy), which were put together by wired rods and wing nuts. The anode and cathode temperature during the operation were measured by two K-type thermocouples, which were connected to a TM-947SD thermometer (max. 1,700 °C, accuracy of 0.1 °C) to read and log the temperature. An electrical circuit including the SOFC-O anode and cathode and a Rigol DL3021 electronic load (0.001 – 40 A) was made to draw and measure the electric current. By connecting cables with alligator clips to the fuel diffuser and the current collector at the top of the Open Flanges Set-up, the electric potential was measured on a UNI-T UT58E multimeter (0.001 – 1,000 V). Finally, a Manson HCS-3202 power supply (1 – 36 V) was used as a booster to compensate for the electric potential loss caused by the electrical resistance of the electrical circuit when drawing an electric current.

The Open Flanges Set-up was placed in a Kittec Squadro SQ11 oven (max. 1,320 °C, accuracy of 1 °C) to control the operating temperature. Calibrated rotameters were used to control the supply of industrial grade pressurised air to the cathode (40 – 800 $mL{\cdot}min^{-1}$) and forming gas, consisting of 5 v% (volume %) H_2 and 95 v% N_2, to the anode (20 – 400 $mL{\cdot}min^{-1}$). The connections of the gas cylinders and connections to the Open Flange Set-up were Swagelok fittings to limit any gas leakages. For the fuel, Acros Organics 25% NH_4OH solution and demineralised water were used to obtain various NH_3-H_2O mixtures. A calibrated Lead Fluid BT101L peristaltic pump (0.001 – 575 $mL{\cdot}min^{-1}$) was used to supply liquid NH_3-H_2O mixtures to the anode. Finally, 1 M HCl solution was used to capture any remaining NH_3 in the anode off-gas. The complete SOFC-O set-up is schematically presented in Fig. 2.

2.2. Methods

2.2.1. Vacuum membrane stripping experiments

For the VMS experiments, feed waters with various initial NH_3 concentrations were prepared by adding NH_4HCO_3 to demi water. NH_4HCO_3 was used as representative salt for residual waters with high

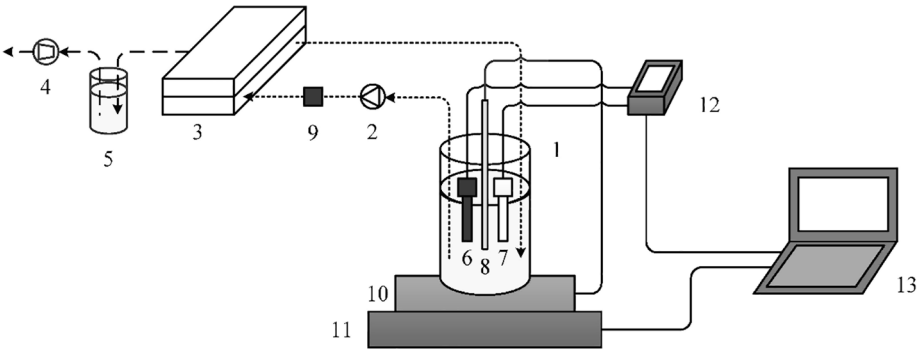

Fig. 1. A schematic representation of the used experimental VMS setup including a feed water bottle (1), peristaltic pump (2), flow-cell including membrane (3), vacuum pump (4), permeate scrubber (5), EC-sensor (6), pH-sensor (7), temperature sensor (8), pressure sensor (9), integrated heating and mixing plate (10), balance (11), multimeter (12) and laptop (13).

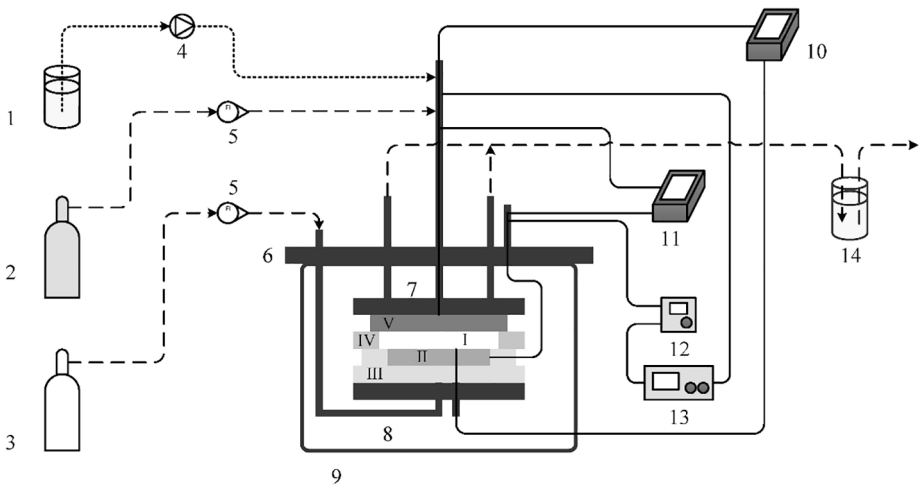

Fig. 2. A schematic representation of the used experimental SOFC setup including a fuel storage bottle (1), forming gas cylinder (2), air cylinder (3), peristaltic pump (4), fuel diffuser (5), Open Flange set-up (6), fuel diffuser (7), air diffuser (8), oven (9), thermometer (10), multimeter for electric potential (11), electric potential booster (12), electronic load (13) and off-gas scrubbing bottle (14). The MEA (I), electric current collector (II), alumina isolation sheets (III), mica sealing sheet (IV) and nickel foam (V) are all placed between the fuel and air diffuser.

TAN concentrations, because bicarbonate (HCO_3^-) is typically the main counter ion of NH_4^+ in residual waters as industrial condensates, sludge reject waters and hydrolysed urine. To obtain NH_3 in the feed water, the solution pH was increased to 10 by adding NaOH to the NH_4HCO_3 solutions.

During the stripping of NH_3 from the feed waters, the NH_3 feed water concentration decreased. By taking samples of the feed water to measure the NH_3 concentration, the NH_3 flux at various NH_3 feed water concentrations was determined. Besides, the H_2O fluxes were determined to assess how much water evaporated along with the stripped NH_3. Based on both the NH_3 and H_2O fluxes, the concentrations of NH_3 in the gaseous VMS permeate as a function of the NH_3 feed water concentration were determined. Next, the effect of the feed water temperature on both the NH_3 and H_2O flux was assessed for feed water temperatures of 25, 35, 45 and 55 °C. For the two mentioned variables, a full factorial design of experiments was set up, and each combination of feed water temperature and NH_3 feed water concentration was assessed in duplicate.

The feed waters were recirculated over the hydrophobic membrane under so-called unsteady hydraulic conditions, corresponding to a Reynolds number of 500 in spacer-filled channels [28]. The pump speed was adjusted accordingly to maintain unsteady conditions for the various feed waters and the cross-flow velocity for the various feed waters ranged between 10 and 20 $cm{\cdot}s^{-1}$. A detailed description of the determination of the cross-flow velocity to obtain unsteady hydraulic conditions based on the feed water characteristics and the dimensions of the flow channel can be found in the Supporting Information (S.I. 1). At the permeate side of the membrane, an absolute pressure of 1.5 kPa was maintained by the vacuum pump. Throughout each run, the total mass, temperature, EC and pH of the feed water were continuously logged and samples were taken every 15 min to measure the NH_3 concentration in the feed water.

2.2.2. Solid oxide fuel cell experiments

When the MEA was installed and the Open Flange Set-up was placed in the oven, the oven temperature was increased at a ramping speed of 120 °C per hour to 400 °C, followed by 200 °C per hour to 750 °C. During the heating of the oven, air was supplied to the cathode at a flow rate of 400 $mL{\cdot}min^{-1}$, while forming gas was supplied to the anode at a flow rate of 200 $mL{\cdot}min^{-1}$ to supply H_2 to gradually reduce NiO to nickel, which catalyses the cracking of NH_3 and the oxidation of H_2. When the oven temperature reached 750 °C, various NH_3-H_2O mixtures were supplied to the anode·NH_3-H_2O mixtures with NH_3 concentrations of 5, 7.5, 10, 12.5 and 25% were prepared by mixing 25 wt% NH_4OH stock solution with demi water. Throughout all experiments, the airflow rate remained 400 $mL{\cdot}min^{-1}$, corresponding to 0.1 mol-$O_2{\cdot}cm^{-2}{\cdot}h^{-1}$, based on an O_2 concentration of 21% in air and an air pressure of 101,325 Pa.

After a stabilisation period of 15 min, the open circuit potential (OCP) was measured for each fuel. Subsequently, the electrical circuit was closed and electric current was drawn in steps of 10 $mA{\cdot}cm^{-2}$. By logging the electric potential measured between the anode and cathode for each electric current step, the peak power density achieved by the SOFC-O for the various fuels was determined. A fuel flow rate of 200 $\mu L{\cdot}min^{-1}$ was used, based on the recommendations of the MEA supplier, which corresponded to an NH_3 flux of 12 $kg{\cdot}m^{-2}{\cdot}h^{-1}$, considering a fuel density ranging from 950 to 986 $g{\cdot}L^{-1}$. Each NH_3 concentration in the fuel was tested in duplicate experiments.

2.3. Performance indicators

2.3.1. Vacuum membrane stripping

The NH_3 and H_2O fluxes were determined using the respective mass differences per unit of membrane area and time (Eq. (4) and Eq. (5), respectively), which were based on the measured feed water masses, NH_3 concentrations, salt concentrations and solution densities at each time instant. A more detailed description of the NH_3 and H_2O mass determination is presented in the Supporting Information (S.I. 2).

$$J_{NH_3} = \frac{-(m_{NH_3,i+1} - m_{NH_3,i})}{A_m \bullet (t_{i+1} - t_i)} \quad (4)$$

$$J_{H_2O} = \frac{-(m_{H_2O,i+1} - m_{H_2O,i})}{A_m \bullet (t_{i+1} - t_i)} \quad (5)$$

where J_{NH_3} and J_{H_2O} = ammonia and water mass flux (in $kg{\cdot}m^{-2}{\cdot}h^{-1}$), $m_{NH_3,i}$ and $m_{H_2O,i}$ = ammonia and water mass at time t_i (in kg), A_m = membrane area (in m^2, $A_m = 0.034\ m^2$) and t_i = time instant 'i' (in h).

Subsequently, the concentration of NH_3 obtained by VMS in the permeate followed from the ratio of the NH_3 flux and the total flux (Eq. (6)).

$$c_{NH_3} = \frac{J_{NH_3}}{J_{NH_3} + J_{H_2O}} \quad (6)$$

where c_{NH_3} = NH_3 concentration in the gaseous VMS permeate (unitless).

The total molar flow rate through the VMS membrane was determined based on the mass flow rates of NH_3 and H_2O (Eq. (7)). Subsequently the volumetric flow rate was determined by using the ideal gas law (Eq. (8)).

$$n_t = \frac{J_{NH_3} \bullet A_m}{MW_{NH_3}} + \frac{J_{H_2O} \bullet A_m}{MW_{H_2O}} \quad (7)$$

$$\frac{Q_{t,in} = n_t \bullet R \bullet T_f}{p_v} \quad (8)$$

where, n_t = total molar flow rate (mol·s^{-1}), MW_{NH_3} and MW_{H_2O} = molecular weight of NH_3 and H_2O, respectively (in g·mol^{-1}, MW_{NH_3} = 17 g·mol^{-1} and MW_{H_2O} = 18 g·mol^{-1}), $Q_{t,in}$ = volumetric gas flow rate (m^3·s^{-1}), R = universal gas constant (in J·mol^{-1}·K^{-1}, R = 8.31 J·mol^{-1}·K^{-1}), T_f = feed water temperature (in K) and p_v = vacuum pressure (in Pa, p_v = 1500 Pa).

The required electrical power for the vacuum pump was determined based on the study of Huttunen et al. [29] (Eq. (9)):

$$\frac{P_{v.p.} = Q_{t,in} \bullet p_v \bullet \ln\left(\frac{p_{atm}}{p_v}\right)}{\eta_{v.p.}} \quad (9)$$

where $P_{v.p}$ = electrical power vacuum pump (in W = J·s^{-1}), p_{atm} = atmospheric pressure (in Pa, p_{atm} = 101,325 Pa = 101,325 kg·m^{-1}·s^{-2}), $\eta_{v.p.}$ = vacuum pump efficiency (unitless, $\eta_{v.p.}$ = 60%).

In addition, we determined the required power of the feed pump to recirculate the feed waters based on the feed flow rate and the measured hydraulic pressure loss over the VMS flow-cell (Eq. (10)).

$$P_{f.p.} = \frac{Q_f \bullet \Delta p_h}{\eta_{f.p.}} \quad (10)$$

where $P_{f.p}$ = electrical power feed pump (in J·s^{-1}), Q_f = flow rate feed pump (in m^3·s^{-1}), Δh = hydraulic pressure loss (in Pa, Δp_h = 15,490 Pa), $\eta_{f.p.}$ = feed pump efficiency (unitless, $\eta_{f.p.}$ = 60%).

At last, the electrical energy consumption for NH_3 stripping from the various feed water at various feed water temperatures and various NH_3 feed water concentration was determined using Eq. (11).

$$E_{VMS} = \frac{P_{v.p.} + P_{r.p.}}{J_N \bullet A_m} \quad (11)$$

where E_{VMS} = energy consumption of VMS to strip NH_3 (in MJ·kg-N^{-1}), J_N = nitrogen mass flux (in kg·m^{-2}·h^{-1}).

2.3.2. Solid oxide fuel cell

For each of the tested fuels, the theoretical Nernst potential was calculated using Eq. (12). The Nernst potential represents the theoretical potential of the oxidation of H_2 (Eq. (3)) after NH_3 cracking in the presence of excess H_2O in the fuel (Eq. (1)).

$$U_{Nernst} = \frac{-\Delta_r G(T)}{N_{e^-,H_2} \bullet F} + \frac{R \bullet T}{N_{e^-,H_2} \bullet F} \bullet ln\left(\frac{[\gamma_{H_2}]^{1.5} \bullet [\gamma_{O_2}]^{0.75}}{[\gamma_{H_2O}]^{1.5+x}}\right) \quad (12)$$

where U_{Nernst} = Nernst potential (in V), $\Delta_r G(T)$ = Gibbs Free Energy of reaction at a certain temperature (in kJ·mol^{-1}, $\Delta_r G$ (750 °C) = −196 kJ·mol^{-1}, lower heating value), T = operating temperature (in K, T = 750 °C = 1023 K), N_{e^-,H_2} = number of electrons per mole of hydrogen during oxidation (unitless, n = 2), F = Faraday constant (C·mol^{-1}, F = 96,485C·mol^{-1}), R = universal gas constant (J·mol^{-1}·K^{-1}, R = 8.31 J·mol^{-1}·K^{-1}), γ_{H_2}, γ_{O_2} and γ_{H_2O} = molar fraction of hydrogen, oxygen and water, respectively (unitless).

Subsequently, the power density, representing the generated electrical power per unit of MEA area, followed from the measured electric potential at a certain electric current (Eq. (15)).

$$p_{SOFC} = \frac{U \bullet I}{A_{MEA}} \quad (13)$$

where p_{SOFC} (in mW·cm^{-2}), U = electric potential (in V), I = electric current (in mA) and A_{MEA} = membrane electrode assemble area (in cm^2, A_{MEA} = 10 cm^2)

Furthermore, the fuel (Eq. (14)) and oxygen utilisation (Eq. (15)) were determined to assess how efficient NH_3 in the fuel and O_2 in the air were used to generate electricity, based on the measured amount of charge (electric current) and the supplied amounts of reactants (H_2 and O_2) for the oxidation of H_2. In addition, the electrical efficiency of the SOFC-O was determined based on the generated power and supplied amount of chemical energy per unit of time (Eq. (15)).

$$\mu_f = \frac{I}{n_{H_2} \bullet N_{e^-,H_2} \bullet} F \quad (14)$$

$$\mu_{O_2} = \frac{I}{n_{O_2} \bullet N_{e^-,O_2} \bullet} F \quad (15)$$

Where μ_f and μ_{O_2} = fuel and oxygen utilisation (unitless), respectively, n_{H_2} and n_{O_2} = molar flow rate of H_2 and O_2, respectively (mol·s^{-1}) and N_{e^-,O_2} = number of electrons per mole of oxygen in the hydrogen oxidation reaction (unitless, n = 4).

$$\eta_{elec} = \frac{p_{SOFC} \bullet A_{MEA}}{n_{H_2} \bullet -\Delta_r G(T)} \quad (16)$$

where, η_{elec} = electrical efficiency (unitless), P = electric power (in W = J·s^{-1}).

Finally, the electrical energy generation of the SOFC-O was calculated using Eq. (17).

$$E_{SOFC-O} = \frac{p_{SOFC} \bullet A_{MEA}}{m_N} \quad (17)$$

where, E_{SOFC-O} = electrical energy generation of the SOFC-O (MJ·kg-N^{-1}).

3. Results and discussion

3.1. Recovery of ammonia-water mixtures by vacuum membrane stripping

3.1.1. Ammonia flux for various feed water temperatures and ammonia feed water concentrations

For the VMS experiments, various feed waters consisting of NH_4HCO_3 at a pH of 10.0 ± 0.1 (average ± standard deviations, n = 17) were prepared. Subsequently, NH_3 was stripped at feed water temperatures of 25, 35, 45 and 55 °C. The deviation in feed water temperature during the experiments was less than 1% of the respective feed water temperature. Due to the addition of NaOH to form dissolved NH_3 in the feed waters, sodium (Na^+), HCO_3^- and carbonate (CO_3^{2-}) ions were also present in the feed waters. The transfer of CO_2 was neglected, because the CO_2 vapour pressure of the feed water was ten times lower than the NH_3 and H_2O vapour pressure of the feed water; at a pH of 10, inorganic carbon is only present as HCO_3^- and CO_3^{2-}.

The reported values of the NH_3 flux in Fig. 3 and the NH_3 feed water concentration for the various feed water temperatures were calculated based on the measured TAN concentration, temperature, pH and ionic strength, and feed water temperature. At a feed water temperature of 25 °C, the NH_3 flux increased from 0.1 to 0.7 kg·m^{-2}·h^{-1} for an increase in NH_3 feed water concentration from 1 to 10 g·L^{-1}. For the same NH_3 feed water concentration range, the NH_3 flux increased from 0.1 to 1.5 kg·m^{-2}·h^{-1} at a feed water temperature of 35 °C, from 0.1 to 1.1 kg·m^{-2}·h^{-1} at 45 °C and from 0.2 to 1.2 kg·m^{-2}·h^{-1} for 55 °C.

For all measured temperatures, the NH_3 flux increased linearly (R^2 = 0.86 – 0.99) as a function of the increasing NH_3 feed water concentration, in line with the studies of El-Bourawi et al. [24] and Scheepers et al. [25]. The linear increase in NH_3 flux as a function of the NH_3 feed water concentration was in contrast to findings of He et al. [20], who found a logarithmic relationship for an NH_3 concentration ranging between 1 and 4 g·L^{-1}, which was probably a result of a high mass transfer resistance, as biogas slurry was used as feed. Henry's Law states that the vapour pressure of dissolved gases in water at a certain temperature is a linear function of the concentration of the respective dissolved gas.

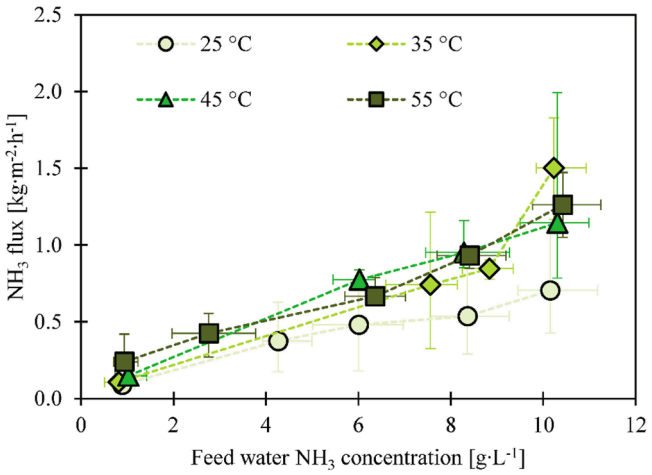

Fig. 3. The NH_3 flux as a function of NH_3 feed water concentration for various feed water temperatures. The vertical error bars represent the minimum and maximum deviations of the measured NH_3 flux of at least triplicate measurements, whereas the horizontal error bars represent the minimum and maximum deviations in the measured feed water NH_3 concentration.

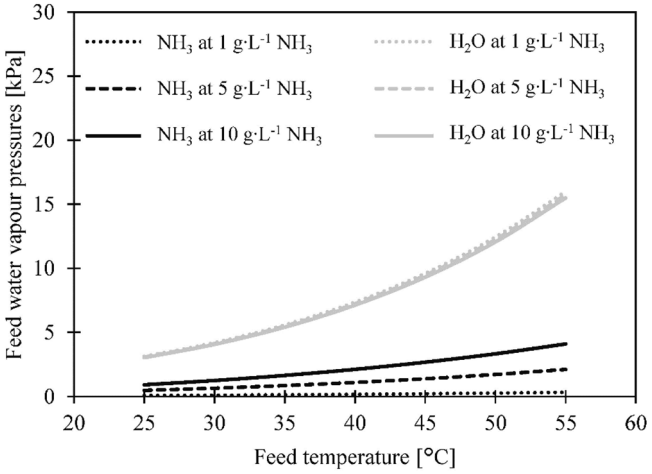

Fig. 4. The NH_3 and H_2O vapour pressure of the feed water as a function of the feed water temperature for various NH_3 feed water concentrations. The vapour pressures were obtained by simulations with PHREEQC software, using the phreeqc.dat database.

Fig. 4 presents the vapour pressures of NH_3 in water as a function of both the feed water temperature and the NH_3 feed water concentration. The vapour pressures of the feed water are obtained by PHREEQC simulation software, taking the NH_3 concentrations, pH, ionic strength and temperature into account to determine chemical equilibria and vapour pressures of solutes (NH_3) and solvent (H_2O). Furthermore, the Dusty Gas Model and Fick's Law, which are applicable for vapour transfer through porous hydrophobic membranes [30], describe that the diffusion flux is linearly proportional to the driving force of gas transfer. Hence, the observed linear increase in NH_3 flux as a function of the NH_3 feed water concentration at each tested feed water temperature was caused by the increase in NH_3 vapour pressure of the feed water. The observed linear increase in NH_3 flux as a function of the NH_3 feed water concentration indicated that the NH_3 mass transfer coefficient remained unaffected, suggesting that no concentration polarisation phenomena affected the NH_3 transfer at increased NH_3 feed water concentrations.

According to Fig. 4, the NH_3 vapour pressure of the feed water increased exponentially with increasing feed water temperatures for a certain NH_3 feed water concentration, which is explained by the temperature dependency of Henry's constant, determined using the van 't Hoff equation, and the decreased solubility of gases for higher feed water temperatures. However, according to Fig. 3, the NH_3 fluxes did not increase consistently as a function of the feed water temperature. The NH_3 fluxes increased when the feed water temperature increased from 25 to 35 °C. However, a further increase in temperature from 35 to 45 and 55 °C, did not result in an increased NH_3 flux. Apparently, when the feed water temperature increased to 45 and 55 °C, the NH_3 mass transfer coefficient decreased, counteracting the increase in NH_3 vapour pressure of the feed water. The decrease in NH_3 mass transfer coefficient over the increasing feed water temperature can be assigned to NH_3 depletion, concentration polarisation, and temperature polarisation, of which the effects become more severe at increased feed water temperatures [20,21]. However, to draw firm conclusions on which polarisation phenomenon affected the NH_3 mass transfer most, more research is required.

3.1.2. *Water flux for various feed water temperatures and ammonia feed water concentrations*

Besides the stripping of NH_3, also evaporation of H_2O through the hydrophobic membrane took place during the VMS experiments. Fig. 5 presents the H_2O flux as a function of the concentration of NH_3 in the feed and the feed water temperature. At a feed water temperature of 25 °C, the H_2O flux decreased from 10 to 7 $kg{\cdot}m^{-2}{\cdot}h^{-1}$ for an increase in NH_3 feed water concentration from 1 to 10 $g{\cdot}L^{-1}$. When the NH_3 feed water concentration increased from 1 to 10 $g{\cdot}L^{-1}$ at a feed water temperature of 35 and 45 °C, the H_2O flux decreased from 16 to 12 $kg{\cdot}m^{-2}{\cdot}h^{-1}$ and from 24 to 22 $kg{\cdot}m^{-2}{\cdot}h^{-1}$, respectively. The H_2O flux at a feed water temperature of 55 °C remained stable at 30 $kg{\cdot}m^{-2}{\cdot}h^{-1}$ as the NH_3 feed water concentration increased from 1 to 10 $g{\cdot}L^{-1}$.

According to Fig. 4, the H_2O vapour pressure of the feed water increased exponentially with the feed water temperature, following the Clausius–Clapeyron relation. However, according to the data, the H_2O flux increased linearly ($R^2 = 0.96 - 1.00$) as a function of the increase in feed water temperature. The observation that the H_2O flux increased linearly while the driving force increases exponentially indicates that the H_2O mass transfer coefficient decreased over the increasing feed water temperature, which might be attributed to temperature polarisation [19,24,31].

According to Fig. 5, the H_2O flux decreased as a function of the increasing NH_3 feed water concentration. For increasing NH_3 in the feed water, increased amounts of NH_4HCO_3 and NaOH were added, resulting

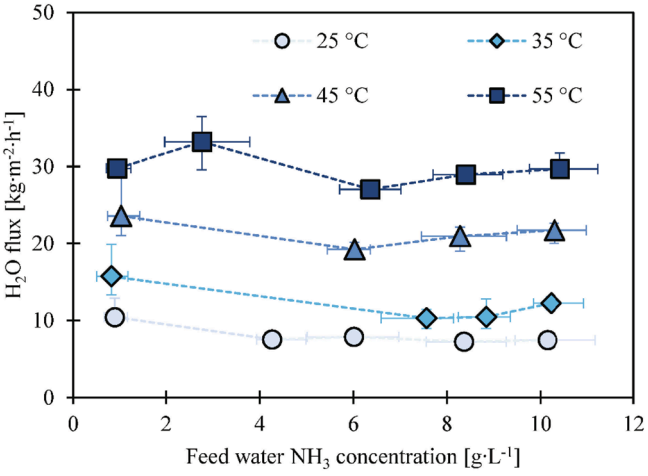

Fig. 5. The H_2O flux as a function of the increasing NH_3 feed water concentration for various feed water temperatures. The vertical error bars represent the minimum and maximum deviations of the measured H_2O flux of at least triplicate measurements, whereas the horizontal error bars represent the minimum and maximum deviations in the measured feed water NH_3 concentration.

in higher ion concentrations during NH_3 stripping. Raoult's Law describes that the vapour pressure of a solvent decreases when the molar fraction of the solutes increases. Based on the data presented in Fig. 4, the H_2O vapour decreased by 3% when the NH_3 concentration increased from 1 to 10 $g{\cdot}L^{-1}$. The decrease in H_2O flux as a function of the increasing NH_3 concentration might also be explained by temperature polarisation, which decreases the H_2O mass transfer coefficient, as described by Martínez-Díez et al. [31].

3.1.3. Ammonia concentration in gaseous vacuum membrane stripping permeate for various feed water temperatures and ammonia feed water concentrations

One of the objectives of this study was to determine the attainable NH_3 concentration in the gaseous VMS permeate for NH_3 reuse purposes. Fig. 6 presents the concentration of NH_3 in the gaseous VMS permeate for the various tested feed water temperatures as a function of the NH_3 feed water concentration. For an increase in the NH_3 feed water concentration from 1 to 10 $g{\cdot}L^{-1}$, the NH_3 concentration in the gaseous VMS permeate increased from 1 to 8 wt% at a feed water temperature of 25 °C. For the same increase in NH_3 feed water concentration, the NH_3 concentration in the gaseous VMS permeate increased from 1 to 11 wt% for a feed water temperature of 35 °C, from 1 to 5 wt% for 45 °C and from 1 to 4 wt% for 55 °C. Hence, increasing the NH_3 feed water concentration resulted in a more NH_3 concentrated gaseous VMS permeate, for all tested feed water temperatures, which can also be derived from the experimental results obtained by Ding et al. [19] and El-Bourawi et al. [24] and the modelling study conducted by Scheepers et al. [25]. The increasing NH_3 concentrations in the gaseous VMS permeate as a function of the increasing NH_3 feed water concentration can be attributed to the increased NH_3 fluxes, while the H_2O flux did not increase.

By increasing the feed water temperature from 25 to 45 and 55 °C, the H_2O flux increased more than the NH_3 flux, leading to more diluted NH_3 in the gaseous VMS permeate, in line with Scheepers et al. [25]. According to Fig. 4, the H_2O vapour pressure of the feed water increases faster than the NH_3 vapour pressure of the feed water as a function of the feed water temperature, which explains the observed higher increase in H_2O flux compared to NH_3 flux as a function of the feed water temperature. Interestingly, by increasing the feed water temperature from 25 to 35 °C, more concentrated NH_3 in the gaseous VMS permeate was obtained, while further increasing the feed water temperature diluted the gaseous VMS permeate. The feed water temperature increase from 25 to 35 °C resulted in a higher increase in NH_3 flux than the increase in H_2O flux. The initial increase in gaseous NH_3 concentration for the feed water temperature increase from 25 to 35 °C can be explained by the combined effect of the various polarisation phenomena: temperature polarisation, accumulated ion concentration polarisation and NH_3 depletion concentration polarisation.

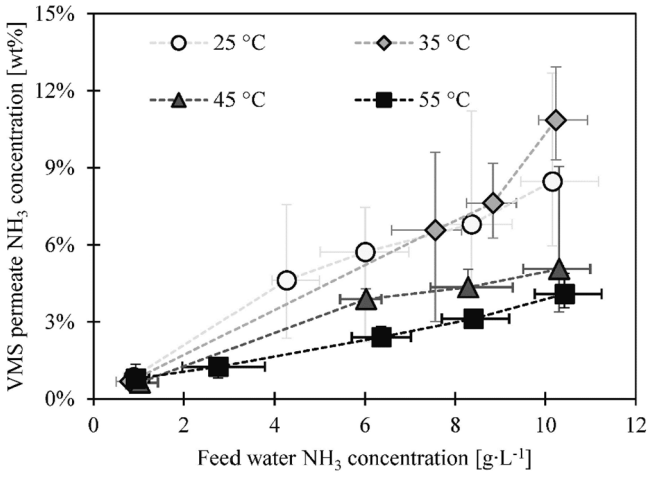

Fig. 6. The concentration of NH_3 in the gaseous VMS permeate as a function of the increasing NH_3 feed water concentration for various feed water temperatures. The vertical error bars represent the minimum and maximum deviations of the measured VMS permeate NH_3 concentrations of at least triplicate measurements, whereas the horizontal error bars represent the minimum and maximum deviations in the measured feed water NH_3 concentration.

3.2. Use of ammonia-water mixtures as fuel for a solid oxide fuel cells

3.2.1. Open circuit potential for various ammonia-water mixtures used as fuel

For the SOFC-O experiments, NH_3-H_2O mixtures with various NH_3 concentrations were prepared. During all experiments, the anode and cathode temperature were stable at 755 and 761 °C, respectively.

Fig. 7A shows the calculated Nernst potential as a function of the NH_3 concentration in the fuel, based on the respective Nernst potential calculation for H_2 oxidation (Eq. (12)), the relevant reactions of NH_3 cracking, and subsequent H_2 oxidation in the presence of H_2O in the fuel (Eq. 1–3). When more NH_3 is present in the fuel, the molar fraction of H_2 at the anode increases, while the molar fraction of H_2O decreases, leading to a higher Nernst potential at a certain temperature.

Fig. 7B shows that by increasing the NH_3 concentration in the fuel from 5 to 25 wt%, the open circuit electric potential increased from 0.82 to 0.93 V. The differences between the measured open circuit electric potential and the calculated Nernst potentials (Fig. 7B) were always below 2% for fuels with 7.5, 10, 12.5 and 25 wt% NH_3, suggesting that even in the presence of excess H_2O, almost complete cracking of NH_3 took place. However, the open circuit electric potential of fuel with 5 wt % NH_3 was unstable throughout the measurements, suggesting that the cracking of NH_3 was affected by the high content of H_2O in this fuel.

According to mass balance calculations based on the amount of supplied NH_3 in the fuel and absorbed in the off-gas scrubber, 95% of the supplied NH_3 in the various fuels was cracked during open-circuit conditions, which is lower than the at least 99.9% reported by Dekker et al. [15] and Ma et al. [16] in absence of H_2O in the fuel. According to Ni et al. [13], the NH_3 cracking efficiency decreases when the partial pressure of NH_3 decreases, explaining the obtained results in our present study.

3.2.2. Generation of electricity using various ammonia-water mixtures as a fuel for solid oxide fuel cell

Fig. 8 presents the measured closed circuit electric potentials and power densities as a function of the current densities for the various fuels in a representative duplicate experiment. In addition, Table 1 presents the average and the minimum and maximum deviations of the peak power density, fuel utilisation, O_2 utilisation and electrical efficiency for the NH_3-H_2O fuels with various NH_3 concentrations in the fuel. The peak power densities, ranging between 114 and 347 $mW{\cdot}cm^{-1}$ were in line with studies in which pure NH_3 was used as a fuel [8,13,14]. According to the results, the peak power density increased as a function of the increasing NH_3 concentrations in the fuel. However, the fuel utilisation decreased when the NH_3 concentration in the fuel increased. Interestingly, the fuel utilisation was 68% when the fuel only contained 5 wt% NH_3, indicating that besides the cracking of NH_3 also subsequent oxidation of H_2 still effectively took place in the presence of high concentrations of H_2O. Hence, although the peak power density of the SOFC-O increased with increasing NH_3 concentrations in the fuel, not all additionally supplied NH_3 resulted in the generation of electricity. To maximise fuel utilisation, all produced H_2 after NH_3 cracking must come in contact with transferred O^{2-} at the triple-phase boundary, which is the interface of the electrolyte, the anode and the electric current collector. However, the O_2 utilisation was at most 31%, suggesting that there was no lack of O_2 supply to the cathode. Therefore, the decrease in fuel utilisation at higher NH_3 concentrations in the fuel was probably caused by less efficient NH_3 cracking, which agrees with the results of

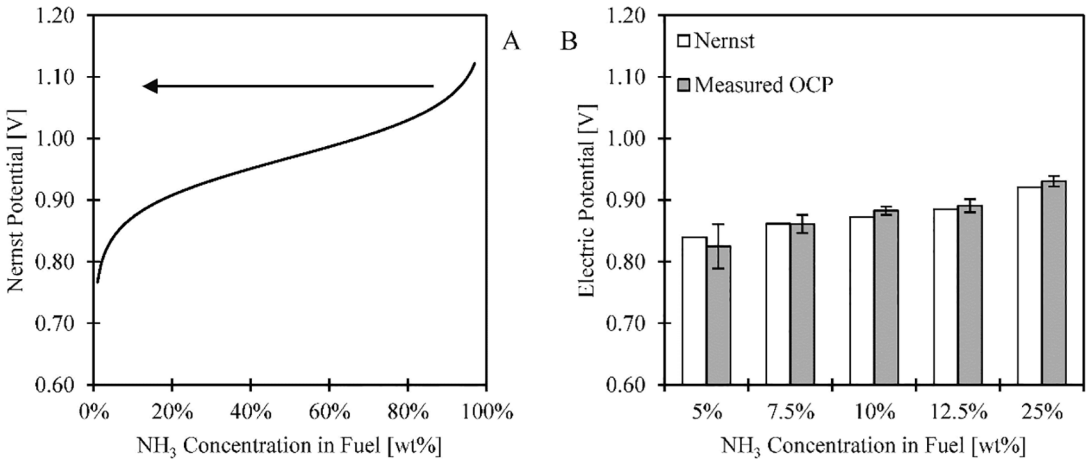

Fig. 7. (A) The Nernst potential as a function of NH_3 concentration in the fuel. The arrow indicates the direction of interpreting the Nernst potential when the fuel becomes diluted with increasing amounts of water (B). The measured open circuit electric potentials and calculated Nernst potentials for the various NH_3 concentrations in the fuel. The vertical error bars represent the minimum and maximum deviations of at least triplicate measurements.

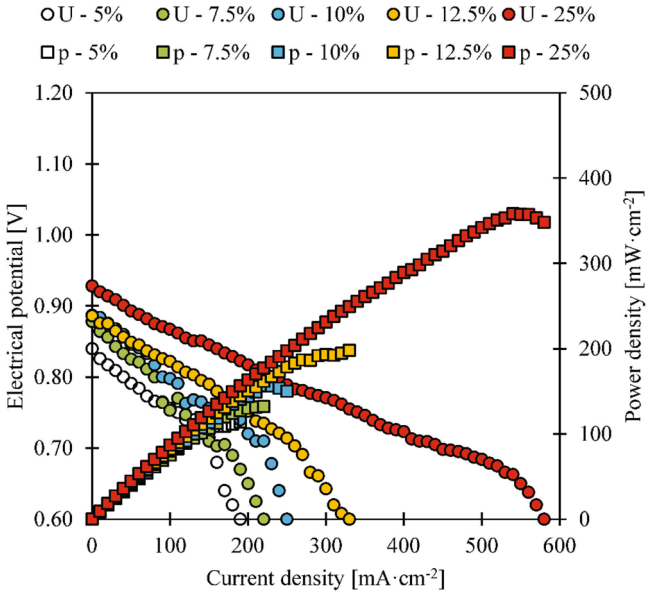

Fig. 8. The measured electric potentials (in circles) and the power densities (in squares) as a function of the generated current density for the tested NH_3-H_2O mixtures with various NH_3 concentrations in wt%.

Table 1
The obtained peak power density, fuel and oxygen utilisation, and the electrical efficiency of the SOFC-O for various concentrations of NH_3 in the fuel. The presented values represent the averages and the minimum and maximum deviations of duplicate measurements.

NH_3 in the fuel	Peak Power Density	Fuel Utilisation	Oxygen Utilisation	Electric Efficiency
wt%	$mW \cdot cm^{-2}$	–	–	–
25	347 ± 11	42 ± 1%	31 ± 1%	27 ± 1%
12.5	212 ± 14	51 ± 3%	19 ± 1%	32 ± 2%
10	157 ± 1	52 ± 7%	16 ± 2%	30%
7.5	138 ± 6	54 ± 1%	12%	35 ± 2%
5	114	68%	10%	43%

Stoeckl et al. [23], who found a similar decrease when more NH_3 was fed to the anode. The electrical efficiency using NH_3-H_2O mixtures with concentrations between 5 and 25 wt% NH_3 as fuel for the SOFC-O ranged between 27 and 43%. According to these results, a SOFC-O can be used to generate electricity, applying NH_3-H_2O mixtures with NH_3 concentrations as low as 5 wt%.

3.3. Energetic evaluation of vacuum membrane stripping and solid oxide fuel cell for the recovery and the use of ammonia

To the best of our knowledge, no previous studies quantified the electrical energy consumption to drive the pumps during the stripping of NH_3 in a VMS configuration, although Scheepers et al. [25] assessed the thermal energy consumption to strip NH_3 by VMS. Notably, residual waters with high TAN concentrations, such as sludge reject water, often already have temperatures in the range of 30–40 °C, because they originate from anaerobic digesters. Therefore, heat addition for VMS may not be needed. Fig. 9 shows the electrical energy consumption for stripping NH_3 from water by VMS as a function of the feed water temperature and the NH_3 feed water concentration. The electrical energy consumption ranged between 84 and 113 $MJ \cdot kg\text{-}N^{-1}$ at an NH_3 feed water concentration of 1 $g \cdot L^{-1}$ and decreased to between 7 and 17 $MJ \cdot kg\text{-}N^{-1}$ when the NH_3 feed water concentration increased to 10 $g \cdot L^{-1}$. The electrical energy consumption was mainly used for the transfer of H_2O water by the vacuum pump. The electrical energy consumption to strip NH_3 decreased with increasing NH_3 feed water

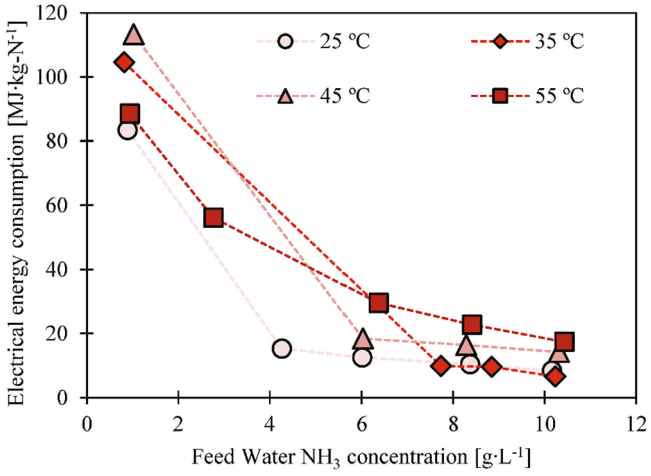

Fig. 9. The calculated average electrical energy consumption to strip NH_3 from water by VMS as a function of the NH_3 concentration for the various feed temperatures.

concentration. The recirculation of the feed water accounted at most for 2% of the electrical energy consumption and can therefore be neglected.

The SOFC-O reached electrical efficiencies ranging between 27% and 43% using NH_3-H_2O mixtures with NH_3 concentrations ranging between 5 and 25 wt%. Based on the determined electrical efficiencies and additional calculations using Eq. (17), the electrical energy generation of the SOFC-O ranged between 6 and 9 MJ·kg-N^{-1}.

Hence, the NH_3 concentrations obtained in the gaseous permeate of VMS reaching up to 11 wt% agreed with the NH_3 concentrations in NH_3-H_2O mixtures that were used for the generation of electricity in an SOFC-O, which were as low as 5 wt%. Moreover, also the electrical energy consumption of VMS of 7 MJ·kg-N^{-1} and the electrical energy generation of the SOFC-O of 9 MJ·kg-N^{-1} aligned, suggesting that the consumed energy of recovering NH_3 from water can be provided by converting the NH_3 to electricity in an SOFC-O.

3.4. Future outlook

This study showed the feasibility of recovering NH_3 from water by VMS as gaseous NH_3-H_2O mixtures with various NH_3 concentrations of up to 11 wt%. However, by better understanding the polarisation phenomena related to ion accumulation, NH_3 depletion and temperature polarisation, transfer of NH_3 may be improved and transfer of H_2O may be suppressed, ultimately leading to higher NH_3 concentrations in the gaseous VMS permeate. According to Fig. 4, the H_2O vapour pressure of the feed water is always higher than the NH_3 vapour pressure of the feed water for the considered operating conditions. Hence, to recover more concentrated NH_3, the use of membranes that suppress permeation of H_2O, while allowing permeation of NH_3 may be explored. To this end, Yang et al. [32] used silica-based pervaporation membranes and reported a remarkable preference for the transfer of NH_3 over H_2O. Moreover, to recover more concentrated NH_3, condensation technologies can be used to condense H_2O, while NH_3 remains in the vapour form, as shown by Fernández-Seara et al. [33].

Furthermore, the minimum NH_3 concentration in NH_3-H_2O mixtures to be used as fuel for an SOFC-O proved to be 5 wt%. It should be noted that the use of fuels with higher NH_3 concentrations resulted in higher power densities, while the electrical efficiency decreased. For the efficient use of SOFC-Os to convert NH_3 in NH_3-H_2O mixtures to electricity, it is important to find an optimum between the power density and electrical efficiency. Therefore, more research is required to optimise the operating conditions, such as fuel flow rate, airflow rate and operating temperature, to achieve higher fuel utilisations, which will lead to higher electrical efficiencies. Besides, based on mass balance calculations using the ingoing and outgoing mass of NH_3, the NH_3 cracking efficiency was at least 95%, while previous literature reported efficiencies higher than 99% using dry NH_3 as fuel for an SOFC-O [15,16]. Interestingly, Stoeckl et al. [22] showed that NH_3 was cracked by at least 99.4% in their SOFC-O stack under open-circuit conditions in the presence of H_2O in the fuel (70 wt% NH_3 and 30 wt% H_2O). Therefore, more research is needed to understand and optimise the cracking of NH_3 in SOFC-Os in the presence of high H_2O content in the fuel (higher than 30 wt%).

4. Conclusions

We showed that NH_3 recovered from water by VMS can be used as a fuel by an SOFC-O. In this study, we assessed the effect of the feed water temperature and the NH_3 feed water concentration on the NH_3 concentration in the obtained gaseous VMS permeate. Besides, we assessed what concentrations of NH_3 in diluted NH_3-H_2O mixtures were suitable for the generation of electricity in an SOFC-O. Finally, we assessed the electrical energy consumption and generation of the respective technologies. Based on the findings, we can conclude the following:

- VMS allowed for the recovery of NH_3 as gaseous NH_3-H_2O mixtures with NH_3 concentrations of 1 – 11 wt% at NH_3 feed water concentration of 1 – 10 g·L^{-1};
- The NH_3 concentration in the gaseous VMS permeate increased when the feed water temperature increased from 25 to 35 °C. However, the NH_3 concentration in the gaseous VMS permeate decreased when the feed water temperature increased to 45 and 55 °C;
- The NH_3 concentration in the gaseous VMS permeate increased as a function of the increasing NH_3 feed water concentration;
- The electrical energy consumption for NH_3 stripping by VMS decreased from 113 to 7 MJ·kg-N^{-1} when the NH_3 feed water concentrations increased from 1 to 10 g·L^{-1}, respectively;
- The SOFC-O generated electricity from NH_3-H_2O mixtures with NH_3 concentrations ranging between 5 and 25 wt%, indicating that NH_3 cracking and subsequent H_2 oxidation still took place in the presence of excess H_2O at the anode;
- The efficiency of cracking NH_3 at the anode was lower than reported in studies that used dry NH_3 as a fuel, suggesting that NH_3 cracking is affected by excess H_2O at the anode;
- The electrical efficiency of the SOFC-O ranged between 27 and 43% and decreased as a function of the increasing NH_3 concentration in the fuel;
- The electrical energy consumption of VMS of 7 MJ·kg-N^{-1} for stripping NH_3 from waters was lower than the electrical energy generation of the SOFC-O of 9 MJ·kg-N^{-1}.

Declaration of Competing Interest

The authors declare that they have no known competing financial interests or personal relationships that could have appeared to influence the work reported in this paper.

Acknowledgements

This study is part of the N2kWh – From Pollutant to Power research (14712), funded by the Netherlands Organisation for Scientific Research (NWO) (former Stichting voor Technische Wetenschappen (STW)); and Agentschap Innoveren & Ondernemen (VLAIO) (former Instituut voor Innovatie door Wetenschap en Technologie (IWT)). We thank the respective funding agencies. In addition, we thank E. Martens and L. Kattenberg for their contributions concerning the execution of the experiments and S. A. Saadabadi for the support concerning the operation of the solid oxide fuel cell.

Appendix A. Supplementary data

Supplementary data to this article can be found online at https://doi.org/10.1016/j.cej.2021.131081.

References

[1] C.M. Mehta, W.O. Khunjar, V. Nguyen, S. Tait, D.J. Batstone, Technologies to recover nutrients from waste streams: A critical review, Crit. Rev. Env. Sci. Technol. 45 (4) (2015) 385–427.
[2] A. Zarebska, D. Romero Nieto, K.V. Christensen, L. Fjerbæk Søtoft, B. Norddahl, Ammonium fertilizers production from manure: A critical review, Crit. Rev. Env. Sci. Technol. 45 (14) (2015) 1469–1521.
[3] Z. Deng, N. van Linden, E. Guillen, H. Spanjers, J.B. van Lier, Recovery and applications of ammoniacal nitrogen from nitrogen-loaded residual streams: A review, Journal of Environmental Management 295 (2021), 113096, https://doi.org/10.1016/j.jenvman.2021.113096. In press.
[4] K. Han, C.K. Ahn, M.S. Lee, C.H. Rhee, J.Y. Kim, H.D. Chun, Current status and challenges of the ammonia-based CO2 capture technologies toward commercialization, Int. J. Greenhouse Gas Control 14 (2013) 270–281.
[5] A. Valera-Medina, H. Xiao, M. Owen-Jones, W.I.F. David, P.J. Bowen, Ammonia for power, Prog. Energy Combust. Sci. 69 (2018) 63–102.
[6] A.B. Stambouli, E. Traversa, Solid oxide fuel cells (SOFCs): a review of an environmentally clean and efficient source of energy, Renew. Sust. Energ. Rev. 6 (2002) 433–455.

[7] D. Cheddie, Ammonia as a Hydrogen Source for Fuel Cells: A Review, in: D. Minic (Ed.), Hydrogen Energy - Challenges and Perspectives, InTech, Rijeka, 2012 pp. Ch. 13.
[8] R. Lan, S. Tao, Ammonia as a Suitable Fuel for Fuel Cells, Front. Energy 2 (2014).
[9] S. Suzuki, H. Muroyama, T. Matsui, K. Eguchi, Fundamental studies on direct ammonia fuel cell employing anion exchange membrane, J. Power Sources 208 (2012) 257–262.
[10] R. Lan, S. Tao, Direct ammonia alkaline anion-exchange membrane fuel cells, Electrochem. Solid-State Lett. 13 (8) (2010) B83, https://doi.org/10.1149/1.3428469.
[11] J. Staniforth, R.M. Ormerod, Clean destruction of waste ammonia with consummate production of electrical power within a solid oxide fuel cell system, Green Chem. 5 (2003) 606–609.
[12] A. Wojcik, H. Middleton, I. Damopoulos, J. Van herle, Van herle, Ammonia as a fuel in solid oxide fuel cells, J. Power Sources 118 (1-2) (2003) 342–348.
[13] M. Ni, M.K.H. Leung, D.Y.C. Leung, Ammonia-fed solid oxide fuel cells for power generation—A review, Int. J. Energy Res. 33 (11) (2009) 943–959.
[14] A. Afif, N. Radenahmad, Q. Cheok, S. Shams, J.H. Kim, A.K. Azad, Ammonia-fed fuel cells: a comprehensive review, Renew. Sust. Energ. Rev. 60 (2016) 822–835.
[15] N.J.J. Dekker, G. Rietveld, Highly efficient conversion of ammonia in electricity by solid oxide fuel cells, J. Fuel Cell Sci. Technol. 3 (2006) 499–502.
[16] Q. Ma, R. Peng, L. Tian, G. Meng, Direct utilization of ammonia in intermediate-temperature solid oxide fuel cells, Electrochem. Commun. 8 (11) (2006) 1791–1795.
[17] T. Okanishi, K. Okura, A. Srifa, H. Muroyama, T. Matsui, M. Kishimoto, M. Saito, H. Iwai, H. Yoshida, M. Saito, T. Koide, H. Iwai, S. Suzuki, Y. Takahashi, T. Horiuchi, H. Yamasaki, S. Matsumoto, S. Yumoto, H. Kubo, J. Kawahara, A. Okabe, Y. Kikkawa, T. Isomura, K. Eguchi, Comparative Study of Ammonia-fueled Solid Oxide Fuel Cell Systems, Fuel Cells 17 (3) (2017) 383–390.
[18] M.S. El-Bourawi, Z. Ding, R. Ma, M. Khayet, A framework for better understanding membrane distillation separation process, J. Membr. Sci. 285 (1-2) (2006) 4–29.
[19] Z. Ding, L. Liu, Z. Li, R. Ma, Z. Yang, Experimental study of ammonia removal from water by membrane distillation (MD): The comparison of three configurations, J. Membr. Sci. 286 (2006) 93–103.
[20] Q. He, G. Yu, T. Tu, S. Yan, Y. Zhang, S. Zhao, Closing CO2 loop in biogas production: recycling ammonia as fertilizer, Environ. Sci. Technol. 51 (2017) 8841–8850.
[21] Q. He, T.e. Tu, S. Yan, X. Yang, M. Duke, Y. Zhang, S. Zhao, Relating water vapor transfer to ammonia recovery from biogas slurry by vacuum membrane distillation, Sep. Purif. Technol. 191 (2018) 182–191.
[22] B. Stoeckl, M. Preininger, V. Subotić, C. Gaber, M. Seidl, P. Sommersacher, H. Schroettner, C. Hochenauer, High Utilization of Humidified Ammonia and Methane in Solid Oxide Fuel Cells: An Experimental Study of Performance and Stability, J. Electrochem. Soc. 166 (12) (2019) F774–F783.
[23] B. Stoeckl, M. Preininger, V. Subotić, S. Megel, C. Folgner, C. Hochenauer, Towards a wastewater energy recovery system: The utilization of humidified ammonia by a solid oxide fuel cell stack, J. Power Sources 450 (2020), 227608.
[24] M.S. EL-Bourawi, M. Khayet, R. Ma, Z. Ding, Z. Li, X. Zhang, Application of vacuum membrane distillation for ammonia removal, J. Membr. Sci. 301 (1-2) (2007) 200–209.
[25] D.M. Scheepers, A.J. Tahir, C. Brunner, E. Guillen-Burrieza, Vacuum membrane distillation multi-component numerical model for ammonia recovery from liquid streams, J. Membr. Sci. 614 (2020), 118399.
[26] N. van Linden, H. Spanjers, J.B. van Lier, Application of dynamic current density for increased concentration factors and reduced energy consumption for concentrating ammonium by electrodialysis, Water Res. 163 (2019) 114856, https://doi.org/10.1016/j.watres.2019.114856.
[27] N. van Linden, G.L. Bandinu, D.A. Vermaas, H. Spanjers, J.B. van Lier, Bipolar membrane electrodialysis for energetically competitive ammonium removal and dissolved ammonia production, J. Clean. Prod. 259 (2020) 120788, https://doi.org/10.1016/j.jclepro.2020.120788.
[28] S.M. Mojab, A. Pollard, J.G. Pharoah, S.B. Beale, E.S. Hanff, Unsteady laminar to turbulent flow in a spacer-filled channel, Flow Turbul Combust 92 (1-2) (2014) 563–577.
[29] M. Huttunen, L. Nygren, T. Kinnarinen, A. Häkkinen, T. Lindh, J. Ahola, V. Karvonen, Specific energy consumption of cake dewatering with vacuum filters, Miner. Eng. 100 (2017) 144–154.
[30] K.W. Lawson, D.R. Lloyd, Membrane distillation, J. Membr. Sci. 124 (1) (1997) 1–25.
[31] L. Martínez-Díez, M.I. Vázquez-González, Temperature and concentration polarization in membrane distillation of aqueous salt solutions, J. Membr. Sci. 156 (2) (1999) 265–273.
[32] X. Yang, T. Fraser, D. Myat, S. Smart, J. Zhang, J. Diniz da Costa, A. Liubinas, M. Duke, A pervaporation study of ammonia solutions using molecular sieve silica membranes, Membranes 4 (1) (2014) 40–54.
[33] J. Fernández-Seara, F.J. Uhía, J. Sieres, Research on the condensation of the ammonia–water mixture on a horizontal smooth tube, Int. J. Refrig 31 (2) (2008) 304–314.